Charge-density analyses of the antiferromagnets NiF_2 and FeF_2 by means of γ-ray diffraction

A. Palmer and W. Jauch
Hahn-Meitner-Institut, Glienicker Strasse 100, 14109 Berlin, Germany
(Received 12 May 1993)

Accurate single-crystal diffraction data have been collected from NiF_2 at room temperature and in the antiferromagnetic state at 15 K, and from antiferromagnetic FeF_2 at 11 K. The γ-ray wavelength used was $\lambda=0.0392$ Å, and the maximum value of $\sin\theta/\lambda$ was 1.40 $Å^{-1}$. Different wavelengths have been applied to correct the strongest reflections of NiF_2 for extinction. On magnetic ordering in NiF_2 a shift of the fluorine ions of 3×10^{-3} Å is found; this confirms a prediction deduced from optical birefringence. In all cases, the centroids of the atomic charge density agree excellently with the nuclear positions determined by neutron diffraction. The static charge density is described by a rigid pseudoatom model; the resulting occupancies of the metal 3*d* orbitals agree with expectations from crystal-field theory; magnetic ordering hardly affects the density deformations in NiF_2. The critical points of the chemical bonds have been determined to obtain information about possible covalency.

I. INTRODUCTION

The antiferromagnetic ordering in NiF_2 has a substantial influence on optical birefringence,[1] and it has been predicted that this is caused by a small internal shift of the fluorine ions.[2] In the magnetically ordered phase of isomorphic MnF_2, neutron and γ-ray experiments yielded different values for the fluorine positional parameter,[3] which has been ascribed to a polarization of the core electron density.[4]

The main purpose of the present study is to accurately determine the centroid of the fluorine electron density in NiF_2 and FeF_2 in order to judge whether the effect of core polarization at the ligands is a general characteristic for this class of antiferromagnets. NiF_2 ($T_N=73$ K) has been investigated both at room temperature (RT) and at 15 K low-temperature (LT), and FeF_2 ($T_N=78$ K) only at 11 K. The fluorine nuclear positions are already known from neutron-diffraction studies,[5] where the same samples had been examined.

The use of an extremely short wavelength has numerous advantages compared with standard x-ray methods: (i) the effects of absorption and extinction are much weaker, (ii) anomalous dispersion does not occur, (iii) the design of sample environment is less complicated, and (iv) reflections of high-momentum transfer are accessible.

Usually, atomic positions and parameters of thermal vibration are determined by least-squares refinements, where the form factors are based on spherical independent-atom models (IAM). In the present work, the influence of the crystal environment on the charge density of the atoms is described quantitatively by multipole parameters of a generalized scattering factor model (GSF); the multipoles can be converted into 3*d*-orbital populations of the transition-metal ions. The chemical bond is discussed in terms of a topological theory developed by Bader and Essén.[6] Additionally, the maximum-entropy method has been applied to the NiF_2 data, but it was found that this "model-free" Fourier inversion is not suited for an accurate determination of the charge density.[7]

II. CRYSTAL STRUCTURE

Like the other transition-metal difluorides, NiF_2 and FeF_2 show the tetragonal rutile-type structure, space group $P4_2/mnm$. The cations are located at 0,0,0; $\frac{1}{2},\frac{1}{2},\frac{1}{2}$, and fluorine at $\pm(x,x,0;\ \frac{1}{2}-x,\frac{1}{2}+x,\frac{1}{2})$. Lattice constants[8,9] are given in Table I. Each metal ion is coordinated by a distorted octahedron of F ions (see Fig. 1). In the antiferromagnetic state of NiF_2 the spins lie slightly canted in the *ab* plane, which results in a weak ferromagnetic moment along *a*, lowering the symmetry to orthorhombic (space group *Pnnm*). In the absence of an external field, the crystal forms [110]-twinned magnetic

TABLE I. Characteristic data of the samples and measurements. The lattice constants are taken from Refs. 8 and 9. For LT NiF_2, the small deviation from tetragonal symmetry amounting to $a-b=1.2\times10^{-3}$ Å has been averaged.

	NiF_2 (298 K)	NiF_2 (15 K)	FeF_2 (11 K)
Lattice constant *a* (Å)	4.6501	4.6478	4.6933
Lattice constant *c* (Å)	3.0835	3.0745	3.3007
Reflection profiles (FWHH in seconds of arc)	12–23	14–25	80–100
Maximum $\sin\theta/\lambda$ ($Å^{-1}$)	1.33	1.33	1.40
No. of reflections	499	519	500
No. of unique reflections	298	267	335

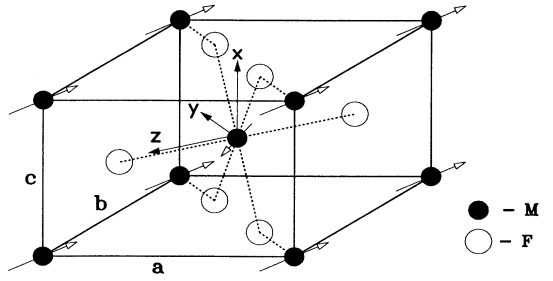

FIG. 1. The rutile-type structure. At LT the spins of NiF_2 lie in the basal plane and are canted to the b axis by a small angle δ. In FeF_2 the spins are parallel to $\pm c$ (not shown here). For the M ion at $(\frac{1}{2},\frac{1}{2},\frac{1}{2})$ the quantization axes x, y, and z are drawn in.

domains, which can be made visible by highly collimated γ radiation.[10] In FeF_2 the spins are parallel to the c axis.

III. EXPERIMENTAL DETAILS

Bragg intensities have been measured on the four-circle γ-ray diffractometer at the Hahn-Meitner-Institut. The most intense line of an ^{192}Ir-source at 0.0392 Å (316.5 keV) was used. The single-crystal specimens were a parallelepiped of NiF_2 ($3.3\times2.8\times1.5$ mm^3) and a prism of FeF_2 (9.4 mm^3). They have been examined by double crystal γ-ray diffraction with a beam divergence of 1.5 sec of arc. The ranges of full width at half height (FWHH) of the intrinsic diffraction profiles for different crystal orientations are given in Table I. The high degree of perfection of the NiF_2 sample gave rise to a particular treatment of the extinction, for which the additional wavelengths 0.0265 and 0.0205 Å were utilized (see Sec. IV).

NiF_2 LT data from an earlier experiment with a multiple-domain sample did not yield satisfactory results in the refinements. Therefore, the data have been recollected in the presence of a static magnetic field generated by coils outside the closed-cycle refrigerator. It has been verified that the field of $\sim$400 Oe along a was sufficient to keep the crystal a single domain.

The vast majority of the reflections have been measured at various ψ settings (rotations about the scattering vector). In the case of a large internal deviation with respect to counting statistics, the corresponding observation was excluded from the refinements. Thus, contamination of the data due to multiple Bragg scattering can be ruled out. The acquisition time was about 3 months for each data set with an initial source activity of 7×10^{12} Bq. Long-time stability has been assured by test reflections, which have proved to be reproducible within 1%.

For an absorption correction of the NiF_2 data the experimentally determined linear absorption coefficient $\mu=0.49(2)$ cm^{-1} was used; this value is in agreement with cross sections given by Hubbel *et al.*[11] For FeF_2, $\mu=0.43$ cm^{-1}. In both crystals, the transmission for different hkl varied by only a few percent and, consequently, any error in μ affects only the scale factor in the structure refinements. In addition, the RT data of NiF_2 have been corrected for isotropic thermal diffuse scattering (TDS); however, the small divergence of the primary beam requires only a narrow ω-scan width (ω being the crystal rotation angle), which limited the maximum contribution of TDS to 3.8% of the Bragg intensity.

IV. EXTINCTION CORRECTION OF NiF_2 DATA

Kinematic theory assumes that only single elastic scattering takes place, and it disregards any loss in intensity as radiation propagates through the crystal. Even if primary extinction is negligible, the rear zone of the crystal may be lighted by a primary beam that is weakened due to diffraction in the front. This apparent absorption, the secondary extinction, becomes more severe the smaller the mosaicity (orientational inhomogeneity) of the sample. In Zachariasen's approximation[12] the transmission factor is

$$y=\frac{|F|^2_{\rm obs}}{|F|^2_{\rm kin}}=(1+2QgT)^{-1/2} \quad (1)$$

with the mean path length of the beam $\bar{T}$ and a mosaic-spread parameter g. For small Bragg angles, the kinematical scattering power per unit volume Q is proportional to λ^2 and hence for moderate extinction (1) may be simplified to

$$y(\lambda)\approx 1-k\lambda^2 .$$

Kinematical structure factors have been obtained by extrapolation to $\lambda=0$ as shown in Fig. 2. The 15 strongest reflections of each NiF_2 data set were measured at three different wavelengths. In all cases where symmetrically equivalent reflections with different mean pathlengths were available, the extrapolation yielded struc-

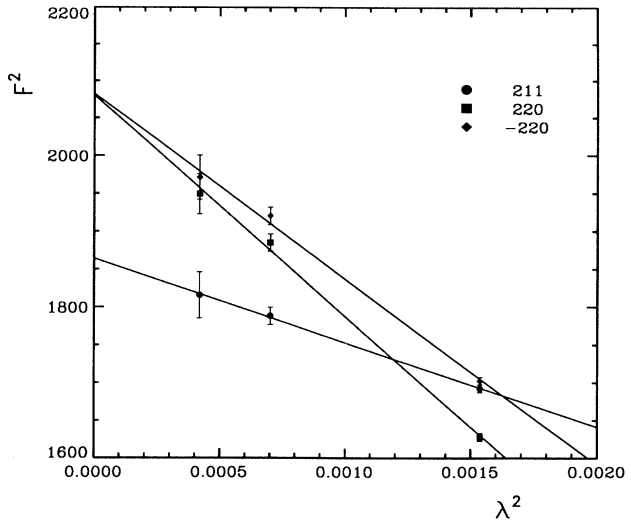

FIG. 2. Examples of strong reflections of NiF_2, measured at three different wavelengths. The values extrapolated to $\lambda=0$ are used in the refinements. For scaling, weak reflections without extinction have been used; they lie on horizontal lines and are not shown here.

ture factors identical within one standard deviation. As a further check for the applicability of this procedure, the slopes of the respective straight lines have been converted into mosaicities. The obtained values are in satisfactory agreement with the experimental rocking curve widths.

In standard x-ray and neutron experiments (where the above approximation is not valid) the extinction correction is part of the structure refinements, yet without any knowledge of the mosaic structure of the sample, which is hardly accessible. In our case, only reflections with $y \geq 0.9$ had to be corrected in the refinements, 96% of them with $y \geq 0.97$. The resulting parameter g is not very well defined and seems to be overestimated by a factor of about 1.5. However, fixing it to the observed average mosaicity has no statistically significant influence on the remaining parameters.

Because of a relatively large mosaic spread, for the FeF_2 sample it was not necessary to pay special attention to the effect of extinction: the refined mosaicity is identical to the observed one.

V. RESULTS

Structure refinements were performed with the program system VALRAY (Ref. 13) minimizing the expression $\sum_i w_i(|F_i^{\rm obs}|^2-|F_i^{\rm calc}|^2)^2$. The test-reflection stability of 1% was used as lower limit for $\sigma(I)/I$; apart from this, the observations were weighted solely by their counting statistical variances: $w_i=\sigma_i^{-2}$. Contrary to common practice in crystallography, no weak reflections [e.g., $I \leq 3\sigma(I)$] have been treated as "unobserved." For all cases considered, the form factors of ions (M^{2+} and F^-) gave statistical indicators slightly better than form factors for neutral atoms.

A. Conventional analysis

The fundamental parameters of the structure have been obtained by least-squares refinements based on an independent-atom model. In the rutile-type structure there is only one free positional parameter x(F), and the thermal vibration tensor of each atom contains three independent components U_{ij}. The expression for the harmonic Debye-Waller factor is

$$W=\exp\left[-2\pi^2\left[U_{11}\frac{h^2}{a^2}+U_{22}\frac{k^2}{a^2}+U_{33}\frac{l^2}{c^2}+2U_{12}\frac{hk}{a^2}\right]\right]$$

with the constraint $U_{11}=U_{22}$. In order to reduce the influence from possible charge-density deformations in the outer shells, high-order refinements were carried out, taking into account only reflections with $\sin\theta/\lambda \geq 0.6$ Å^{-1}; the results are given in Table II. Furthermore, NiF_2 LT data have been evaluated based on the orthorhombic space group *Pnnm*, where the constraints $x=y$ and $U_{11}=U_{22}$ are not valid. However, these refinements confirmed the results of neutron diffraction:[5] the fluorine ions remain on the diagonals and the difference in the thermal parameters U_{11} and U_{22} is insignificant for both atoms. Hence, it seems justified to neglect the small deviation from tetragonal symmetry. Since the x parameters are in good agreement with those obtained from neutron diffraction, there is no evidence for a polarization of the fluorine electron density.

B. Analysis with generalized structure factors

The charge density has been modeled within the concept of rigid pseudoatoms as given by Stewart.[14] Here, the atoms are partitioned into a frozen core and a variable valence shell. The valence density is described by a multipole expansion up to fourth order, a radial scaling parameter κ, and a population parameter P_{00} that allows for charge transfer between different atoms, under the constraint of a neutral unit cell.

The radial density functions were based on canonical Hartree-Fock wave functions, taken from Clementi and Roetti.[15] The multipoles on M^{2+} were constructed from $3d3d$ orbital products. On F^-, the dipole and quadrupole terms were based on $2s2p$ and $2p2p$ products, respectively; for the higher multipoles with $l=3,4$ Slater-type functions with a fixed orbital parameter[15] $\alpha=5.1$ a.u.$^{-1}$ were used. Point symmetry restricts the number of independent multipole parameters to two quadrupoles and three hexadecapoles on both M and F positions. Additionally, there are one dipole and two octopoles allowed

TABLE II. Results of high-order refinements with $\sin\theta/\lambda \geq 0.6$ Å^{-1}. $wR(F^2)=[\Sigma w(F_{\rm obs}^2-F_{\rm calc}^2)^2/\Sigma wF_{\rm obs}^4]^{1/2}$; goodness of fit $=[\Sigma w(F_{\rm obs}^2-F_{\rm calc}^2)^2/(N_{\rm obs}-N_{\rm param})]^{1/2}$. Standard deviations (in parentheses) refer to the last digits given. The x parameters from neutron diffraction are taken from Ref. 5.

		NiF_2 (298 K)	NiF_2 (15 K)	FeF_2 (11 K)
	$wR(F^2)$	0.029 6	0.030 9	0.029 6
	goodness of fit	1.254	1.577	1.444
M:	U_{11} (Å^2)	0.005 81(2)	0.002 57(2)	0.002 07(3)
	U_{33}	0.004 85(4)	0.002 48(3)	0.001 65(3)
	U_{12}	−0.000 17(12)	−0.000 07(11)	−0.000 39(11)
F:	x	0.303 64(9)	0.303 26(8)	0.301 21(8)
	U_{11} (Å^2)	0.010 31(12)	0.004 83(8)	0.004 30(8)
	U_{33}	0.007 29(19)	0.004 05(13)	0.003 45(12)
	U_{12}	−0.004 46(15)	−0.001 47(11)	−0.001 44(11)
	$x_{\rm neutrons}$	0.303 65(4)	0.303 32(4)	0.301 20(4)

on F. The local coordinate system is chosen as shown in Fig. 1: the z axis lies along the short $M-F$ bond in the [110] direction, and x is parallel to the crystallographic c axis.

Since information about possible anharmonic thermal motion of the nuclei is not presently available, it is difficult to separate deformations of the pseudoatom from the effect of any anharmonic potential. Therefore, data have also been analyzed with an IAM, where the Debye-Waller factor was expanded into a Gram-Charlier series[16] up to terms of fourth order. However, the poor significance of the anharmonic parameters (especially in high-order refinements) and their inconsistent temperature dependence led to the conclusion that the statistical improvement compared with conventional refinements is mainly a result of modeling outer-shell deformations by anharmonic parameters. Thus, we consider a harmonic potential to be sufficient for describing the thermal motion.

In Table III the results for the GSF models are listed. The six population parameters of the M ions, P_{00} and the five multipoles, are converted into $3d$ occupancies by a (6×6) matrix similar to the one derived by Holladay, Leung, and Coppens.[17] Insignificant multipoles on the fluorine ion and the values for κ, which do not significantly differ from 1, are not itemized. The U_{ij} are almost identical to those of Table II, which indicates that they are sufficiently decorrelated from the effect of asphericities. It has been verified that the total model charge density stays positive throughout the unit cell.

Figure 3 shows static deformation densities from the GSF models, i.e., the density contributions of multipoles with $l \geq 1$ calculated in direct space. The charge depletion at the metal ions in the ligand directions is well recognizable, and so is the interstitial enhancement. Obviously, in FeF_2 the asphericities on F are not significant.

C. Topology of the charge density

In this section the charge density is discussed in terms of the theory developed by Bader and Essén.[6] The model density of pseudoatoms $\rho(\mathbf{r})$ is calculated in direct space and deconvoluted from thermal motion. Figure 4(a) shows a map of the total charge density in the (110) plane of RT NiF_2. The Laplacian of $\rho(\mathbf{r})$ has negative values in regions where there is a local excess of density and it is positive in regions of local depletion. The $-\nabla^2\rho$ map in Fig. 4(b) exhibits more details of the density; the shell structures and a relative depletion at the Ni ion in the ligand directions are plainly visible.

The Laplacian of ρ also provides a quantitative criterion for a description of chemical bonds. It may be written as

$$\nabla^2\rho(\mathbf{r})=\frac{\partial^2\rho}{\partial x_1^2}+\frac{\partial^2\rho}{\partial x_2^2}+\frac{\partial^2\rho}{\partial x_3^2}=\lambda_1+\lambda_2+\lambda_3$$

with the principal curvatures λ_i. The atomic interaction can be characterized by the sign of the Laplacian at a bond critical point $\mathbf{r}_c$, where the gradient of $\rho(\mathbf{r})$ is zero and the sum of the signs of λ_i is -1. $\nabla^2\rho(\mathbf{r}_c)<0$ indicates covalent interaction, $\nabla^2\rho(\mathbf{r}_c)>0$ closed-shell (or ionic) interaction. In the following, λ_3 denotes the positive curvature along the bond direction. The two negative curvatures are perpendicular to the bond.

In Table IV the density, its Laplacian, and its three principal curvatures at the bond critical points are given for both the IAM and the GSF model. The IAM model reveals the expected ionic bond character with a low density at the critical point where λ_3 strongly overweighs $(\lambda_1+\lambda_2)$. Allowing for multipole deformations has a rather small influence on the total $\nabla^2\rho(\mathbf{r})$; in NiF_2 the density tends to decrease and the individual curvatures

TABLE III. Results for the GSF models. The multipole parameters of F are given in units of their standard deviation if they exceed 1σ.

		NiF_2 (298 K)	NiF_2 (15 K)	FeF_2 (11 K)
	$wR(F^2)$	0.024 7	0.022 0	0.024 8
	goodness of fit	1.250	1.247	1.334
M:	U_{11} (Å^2)	0.005 88(3)	0.002 63(2)	0.002 06(2)
	U_{33}	0.004 70(6)	0.002 29(3)	0.001 68(3)
	U_{12}	−0.000 24(19)	−0.000 01(15)	−0.000 07(13)
	P_{00}	7.81(7)	8.02(7)	5.92(5)
	d_{z^2}	0.91(11)	0.94(8)	1.15(12)
	d_{xy}	1.03(13)	1.24(9)	1.04(13)
	d_{xz}	1.77(10)	1.89(8)	0.88(11)
	d_{yz}	2.01(10)	1.88(8)	0.95(11)
	$d_{x^2-y^2}$	2.09(12)	2.07(9)	1.90(13)
F:	x	0.303 67(11)	0.303 21(7)	0.301 28(10)
	U_{11} (Å^2)	0.010 14(16)	0.004 73(8)	0.004 34(12)
	U_{33}	0.007 17(28)	0.003 99(14)	0.003 50(20)
	U_{12}	−0.003 89(24)	−0.001 22(12)	−0.001 63(21)
	$Q_{x^2-y^2}$	1.4σ		
	Q_{z^2-1}	-2.9σ	-2.5σ	
	$H_{x^2y^2z^2}$			-2.3σ

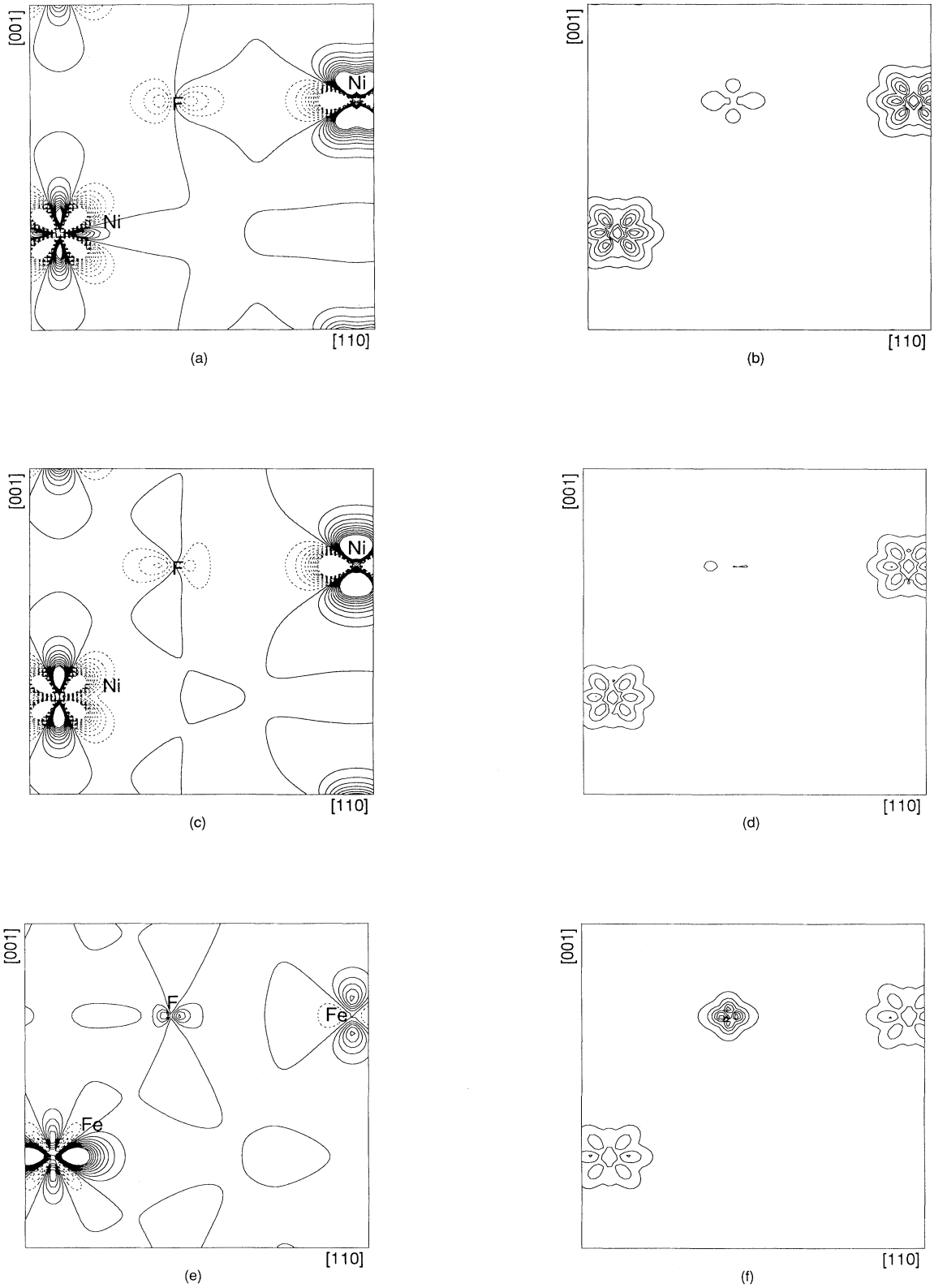

FIG. 3. Density contribution from multipoles with $l \geq 1$ in a (3.8 Å × 3.8 Å) area of the (110) plane. (a) NiF_2 at RT with error map (b); (c) and (d) NiF_2 at LT; (e) and (f) FeF_2. Solid lines represent positive (and zero) regions, dashed lines negative regions in steps of ± 0.25 eÅ^{-3}. The densities are truncated at ± 2.5 eÅ^{-3}.

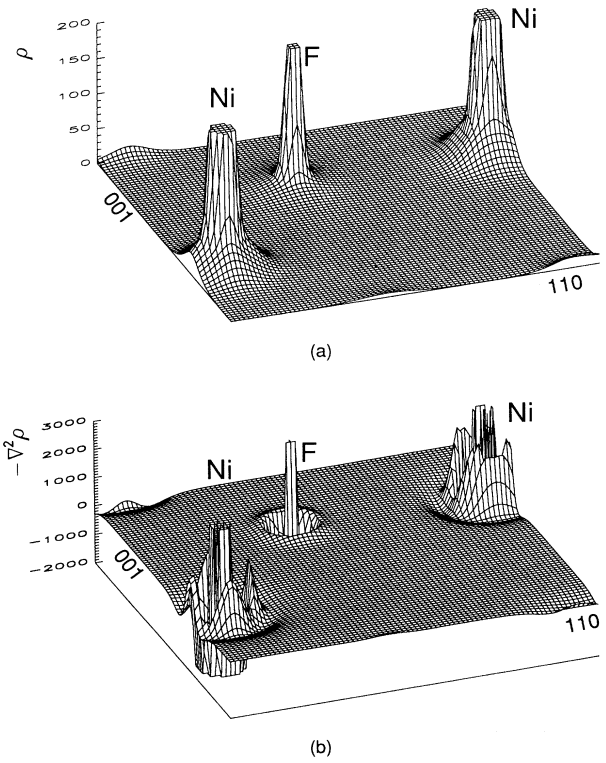

FIG. 4. The calculated total density in the (110) plane of NiF_2 at RT (a) and its negative Laplacian (b). The truncated values are given in $e\text{Å}^{-3}$ and $e\text{Å}^{-5}$, respectively.

become smaller. The ellipticity $\epsilon=\lambda_1/\lambda_2-1$ is almost zero for NiF_2, indicating that there is no π contribution in the bonds.

VI. DISCUSSION

In NiF_2, a small change in the fluorine positional parameter has been observed. The magnetostrictive shift of $\Delta x = x(\mathrm{RT}) - x(\mathrm{LT}) = 4\times10^{-4}$ agrees both in sign and magnitude with the predicted value of 4.5×10^{-4} that was deduced from optical birefringence.[2]

From comparison with nuclear positions from neutron diffraction, neither in NiF_2 nor in FeF_2 is there any indication for a polarization of the fluorine electrons. Although one may in general expect the center of the core electrons to coincide exactly with the nuclear position, the achieved experimental agreement down to the order of 10^{-4} Å is not self-evident; it demonstrates the capacity of combining γ ray and neutron diffraction, which, on the other hand, has revealed a discrepancy of 1.5×10^{-3} Å in the antiferromagnetic phase of MnF_2. Despite the small influence of magnetic order on the charge density in NiF_2 one may consider MnF_2 a special case because of the highly symmetrical $3d^5$ configuration of the Mn^{2+} ion, which might restrict asphericities to being located only on the ligands.

The problem of extinction has been solved for the NiF_2 crystal by using three different γ wavelengths. This yielded reliable low-order reflections, which determine the electron density in the outer shells of the atoms. The use of generalized scattering factors led to $3d$-occupancies, which come up to the expectations for octahedrally coordinated transition metal ions, even though restrictions like the Pauli principle or a fixed value for the total $3d$ population have not been imposed.

For the $3d^6$ high-spin configuration of the Fe^{2+} ion, one of its t_{2g} orbitals should be occupied by two electrons. The threefold degeneracy of the t_{2g} terms is lifted by the slight distortion of the F octahedron, so that $E(d_{yz}) > E(d_{xz}) > E(d_{x^2-y^2})$.[18] Our diffraction data unequivocally implicate the twofold occupancy of the orbital of lowest energy, whereas x-ray diffraction experiments by de Almeida, Costa, and Paixao[19] only indicate preference for the xy plane. This might be caused by a high correlation between thermal and multipole parameters due to their $\sin\theta/\lambda$ limit of 1.08 Å^{-1}. Since our data sets are much more extended, the multipoles are less influenced by this kind of correlation.

TABLE IV. Bond critical points, derived from the IAM and the GSF models. Values of ρ in $e\text{Å}^{-3}$, values of $\nabla^2\rho$ and λ_i in $e\text{Å}^{-5}$. No standard deviations are given for the IAM models, since here no density parameters have been varied.

		x	y	z	ρ	$\nabla^2\rho$	λ_1	λ_2	λ_3
NiF_2									
RT, short	IAM	0.152	0.152	0.000	0.44	10.4	−2.4	−2.4	15.2
	GSF	0.148	0.148	0.000	0.34(2)	10.5(2)	−1.2	−1.0	12.7
LT, short	IAM	0.152	0.152	0.000	0.44	10.5	−2.5	−2.4	15.4
	GSF	0.148	0.148	0.000	0.36(1)	10.7(1)	−1.5	−1.0	13.2
RT, long	IAM	0.402	0.402	0.250	0.42	9.9	−2.3	−2.3	14.5
	GSF	0.410	0.410	0.246	0.37(1)	10.3(1)	−1.6	−1.4	13.2
LT, long	IAM	0.402	0.402	0.250	0.42	10.0	−2.3	−2.3	14.6
	GSF	0.407	0.407	0.246	0.39(1)	10.4(1)	−1.9	−1.6	13.9
FeF_2									
short	IAM	0.141	0.141	0.000	0.28	9.3	−1.7	−1.7	12.8
	GSF	0.140	0.140	0.000	0.28(2)	9.2(2)	−2.3	−1.7	13.1
long	IAM	0.409	0.409	0.268	0.20	6.5	−1.1	−1.1	8.7
	GSF	0.411	0.411	0.270	0.19(1)	7.2(1)	−1.2	−0.6	9.0

From polarized neutron diffraction and *ab initio* calculations of spin densities in the local density approximation, Brown, Figgis, and Reynolds[20,21] arrive at models for which $P_{00}(\mathrm{Ni})=8.31$ (populations of $d_{z^2}=1.22$ and $d_{xy}=1.17$) and $P_{00}(\mathrm{Fe})=6.15$ ($d_{z^2}=1.13, d_{xy}=1.08$). They obtain a spin delocalization of 28% from Ni to F (10% from Fe to F) and conclude that this indicates a very large amount of "covalency" in compounds that traditionally are thought to be ionic. It should be emphasized that we did not refine orbital populations and especially not those of bond orbitals. Rather, we have modeled a given shape of charge distribution by multipoles, which have been converted afterwards into $3d$ occupancies (this procedure presupposes negligible overlap and a $3d3d$ representation of the valence shell). When using the GSF model instead of the IAM, the calculated density in the Ni-F bond should be substantially reduced, since for a spherical Ni ion all the $3d$ orbitals are occupied by 8/5 electrons, whereas each e_g orbital of the nonspherical ion contains only one electron. However, the decrease in charge at the bond critical points is small and all the curvatures of $\rho(\mathbf{r})$ become smoother, which may reflect a considerable covalent contribution. Nevertheless, in terms of charge density the bond character is doubtless "ionic." In FeF_2 there is no effect on $\rho(\mathbf{r}_c)$; this may be due to the small difference between 6/5 and 1 being compensated by a slight covalency. The ellipticities reflect the strong deformation of the Fe $3d$ shell arising from the twofold occupancy of the $d_{x^2-y^2}$ orbital. They can not be ascribed to a contribution from π bonding, since asphericities of the F ion are not significant.

Recently, Dufek, Schwarz, and Blaha[22] have performed band-structure calculations of NiF_2 with a full potential linearized-augmented-plane-wave method. They obtain a deformation density which is qualitatively similar to that in Fig. 3 and they note that the covalent contribution to the bond is of σ rather than of π character. This agrees with our result from the small ellipticity of the charge density at the critical points.

In conclusion, extended accurate γ-ray-diffraction data enabled us to analyze details of the charge density in NiF_2 and FeF_2. The short wavelength allowed use of the same samples as in neutron experiments; the positional parameters of the complementary methods are in excellent agreement, denying a polarization of the fluorine ions. The $3d$ occupancies confirm the expectations from crystal-field theory, whereas indications for covalency in the chemical bonds cannot be directly corroborated.

ACKNOWLEDGMENTS

We wish to thank Professor R. F. Stewart for helpful discussions and for making the program VALRAY available to us. We are grateful to Dr. I. R. Jahn for the loan of the samples.

[1]I. R. Jahn, Phys. Status Solidi B **57**, 681 (1973).
[2]W. Jauch, Phys. Rev. B **44**, 6864 (1991).
[3]W. Jauch, G. J. McIntyre, and A. J. Schultz, Acta Crystallogr. B **46**, 739 (1990).
[4]W. Jauch and R. F. Stewart (unpublished).
[5]W. Jauch, A. Palmer, and A. J. Schultz, Acta Crystallogr. B (to be published).
[6]R. F. W. Bader and H. Essén, J. Chem. Phys. **80**, 1943 (1984).
[7]W. Jauch and A. Palmer, Acta Crystallogr. A **49**, 590 (1993).
[8]K. Haefner, J. W. Stout, and C. S. Barrett, J. Appl. Phys. **37**, 449 (1966).
[9]K. Haefner, Ph.D. thesis, University of Chicago, 1964.
[10]A. Palmer and W. Jauch, Solid State Commun. **77**, 95 (1991).
[11]J. H. Hubbel, W. J. Veigele, E. A. Briggs, R. T. Brown, D. T. Cromer, and R. J. Howerton, J. Phys. Chem. Ref. Data **4**, 471 (1975).
[12]W. H. Zachariasen, Acta Crystallogr. **23**, 558 (1967).
[13]R. F. Stewart and M. A. Spackman (unpublished).
[14]R. F. Stewart, Acta Crystallogr. A **32**, 565 (1976).
[15]E. Clementi and C. Roetti, At. Data Nucl. Data Tables **14**, 177 (1974).
[16]See, for example, U. H. Zucker and H. Schulz, Acta Crystallogr. A **38**, 563 (1982).
[17]A. Holladay, P. Leung, and P. Coppens, Acta Crystallogr. A **39**, 377 (1983).
[18]R. Reschke, A. Trautwein, and F. E. Harris, Phys. Rev. B **15**, 2708 (1977).
[19]M. J. M. de Almeida, M. M. R. Costa, and J. A. Paixao, Acta Crystallogr. B **45**, 549 (1989).
[20]P. J. Brown, B. N. Figgis, and P. A. Reynolds, J. Phys.: Condens. Matter **2**, 5297 (1990).
[21]P. J. Brown, B. N. Figgis, and P. A. Reynolds, J. Phys.: Condens. Matter **2**, 5309 (1990).
[22]P. Dufek, K. Schwarz, and P. Blaha, Phys. Rev. B (to be published).